Deterministic transport in biased maps: Crossover from dispersive to regular transport

E. Barkai[1] and J. Klafter[2]
[1]School of Physics and Astronomy, Beverly and Raymond Sackler Faculty of Exact Sciences, Tel Aviv University, Tel Aviv 69978, Israel
[2]School of Chemistry, Beverly and Raymond Sackler Faculty of Exact Sciences, Tel Aviv University, Tel Aviv 69978, Israel
(Received 12 June 1997)

We investigate the influence of a weak uniform field ϵ on chaotic diffusion generated by iterated maps which, in the absence of the field, lead to subdiffusion. When $\epsilon=0$, the probability density $\psi(t)$ of the escape times from the vicinity of the fixed points of the maps decays as a power law. When a field is switched on, $\psi(t)$ decays exponentially at long enough times, with a decay rate that diverges when ϵ becomes small. The mean displacement and mean squared displacement show a transition from an anomalous type of motion, valid at short times, to a normal behavior at long times. [S1063-651X(98)11404-6]

PACS number(s): 05.45.+b, 05.40.+j, 05.60.+w, 02.50.−r

I. INTRODUCTION

Deterministically generated normal and anomalous diffusion are by now well established. Simple theoretical tools which lead to such diffusional processes are one-dimensional iterated maps, which generate sets of trajectories according to an iteration rule $x_{n+1}=g(x_n)$ [1–6]. Most of the existing works have concentrated on maps which have the symmetry properties

$$g(x)=-g(-x) \quad \text{and} \quad g(x+N)=g(x)+N, \tag{1}$$

with N being an integer. Averaging over initial conditions one obtains the mean squared displacement

$$\langle x^2(t)\rangle \sim t^{\delta}, \tag{2}$$

where the exponent δ depends on a single parameter of the maps [3, 4]. Depending on δ, Eq. (2) describes subdiffusion, also referred to as dispersive diffusion ($\delta<1$), normal diffusion ($\delta=1$), or enhanced diffusion ($\delta>1$). It has been shown that the statistical properties of the trajectories generated by these maps are well described by random walk models, especially by continuous time random walks (CTRW's) [3–8]. The symmetry properties of the previously considered maps guarantee that, for properly chosen initial conditions, no drift exists, so that $\langle x(t)\rangle=0$.

In spite of their simplicity one-dimensional iterated maps provide a useful description and understanding of complex motion with trajectories that resemble those observed in experiments. Geisel, Nierwetberg, and Zacherl [4] applied such a map to model diffusion in Josephsons junctions. Reference [8] considered a one-dimensional map that generates intermittent chaotic motion with both dispersive and enhanced modes of diffusion. Similar behavior has been found in a recent experiment by Solomon, Weeks, and Swinney [9] on tracer particles in a two-dimensional rotating flow. It has been observed that under certain conditions the tracer particles perform long flights but are intermittently trapped in space for long times. Direct measurements show that both the flight times and trapping times are distributed according to power laws. Recently, Weeks, Urbach, and Swinney [10] applied a bias to the tracer particles, and measured the drift as well as the trapping and flight times. It is therefore of interest to investigate maps under bias, and find whether they can be useful in describing biased transport of particles.

Here we consider the transport properties of particles subject to biased maps. We add a weak uniform bias ϵ to a map, which otherwise behaves subdiffusively, and calculate different features of the response to the external field. The field which acts on the system from one end to the other in a uniform way, breaks the symmetry of the system. Previous works considered three other types of fields which break the symmetry of the map $g(x)$. These include environmental fluctuations (time dependent noise) [11], quenched disorder (time independent) [12] and the so called geometric and dynamical bias [13–15], for which the enhanced diffusion regime was investigated. The first two cases did not lead to a net drift, while the third case produces a drift. The perturbations considered by Trefán and co-workers [13–15] are very different from the field introduced here. Similarities and differences between our and previous results will be discussed briefly in the last section. Two topics are addressed in this paper.

(1) The time evolution of x_n on short length scales. It has been shown that slow diffusion is caused by particles which are trapped for long periods of time close to unstable fixed points of the map [3]. We study the statistical nature of the escape times from points in the vicinity of a fixed point across a fixed boundary. Especially, we would like to know the dependence of the these times on the external field. An interesting result is that the power law dependence of the probability density function (p.d.f.) of the escape times, characteristic of the $\epsilon=0$ case, crosses over to an exponential behavior in the presence of a field. Hence, this p.d.f. is sensitive to the external bias.

(2) The evolution on longer length scales. When a bias exists the symmetry of the map is broken, and a drift occurs. Among other things we show that for small but finite ϵ, $\langle x(t)\rangle_{\epsilon}$ increases linearly with time at long times. We also show that for any finite ϵ there exists a time after which the mean squared displacement increases linearly with time. The transport behaves anomalously for short times and then crosses over to a normal type of behavior.

II. DISPERSIVE MOTION

Geisel and Thomae [3] introduced a one-dimensional map for which the mean squared displacement behaves subdiffu-

sively. Following this work, a similar map was considered in Ref. [5], and the corresponding probability distribution $P(x,t)$ to be at location x at time t was calculated. They demonstrated that the CTRW is a valid stochastic description of the diffusion processes which are the outcome of these deterministic maps.

The biased map considered here is

$$x_{n+1}=g(x_n)+\epsilon, \tag{3}$$

where $g(x)$ has a periodic shift symmetry and inversion antisymmetry [Eq. (1)]. The weak bias ϵ, introduced here, breaks the antisymmetry of the system. Using Eqs. (1) and (3), the definition of $g(x)$ is required only in the range $0 \leqslant x < \frac{1}{2}$. Following Ref. [16], one decomposes the coordinate x_n into a box number N_n and the position $0<\tilde{x}_n<1$ within the box,

$$x_n=N_n+\tilde{x}_n. \tag{4}$$

Thus the box number N_n and reduced coordinate $\tilde{x}_n$ are iterated according to

$$\tilde{x}_{n+1}=\tilde{g}_\epsilon(\tilde{x}_n),$$

$$N_{n+1}=N_n+\hat{g}_\epsilon(\tilde{x}_n), \tag{5}$$

where $\tilde{g}_\epsilon(\tilde{x})$ is the reduced map for the reduced coordinate $\tilde{x}$, and $\hat{g}_\epsilon(\tilde{x})$ is used to increment or decrement the box number N.

Geisel and Thomae [3] considered a rather wide family of maps which behave as

$$g(x)=(1+\lambda)x+ax^z \quad \text{for } x\to+0 \tag{6}$$

where $\lambda \ll 1$ and $z>1$. We use a map which belongs to this family [5],

$$g(x)=x+ax^z, \quad 0\leqslant x<\frac{1}{2} \tag{7}$$

with $a=2^z$. In Fig. 1, we show the map $g(x)+\epsilon$ for three boxes. Notice that the bias shifts the fixed points from their $\epsilon=0$ integer values.

Consider first the case $\epsilon=0$ which was investigated previously. The probability density of the residence time in a cell, for $\lambda\to 0$, is [3]

$$\psi(t)=\frac{2a}{[2^{z-1}+a(z-1)t]^{z/(z-1)}}, \tag{8}$$

displaying a power law behavior. The normalized function Eq. (8) is used within the framework of the CTRW to calculate $P(x,t)$ and $\langle x^2(t)\rangle$ [5]. Setting $\gamma \equiv 1/(z-1)$ one finds, for $t\to\infty$,

$$\langle x^2(t)\rangle \sim \begin{cases} t^\gamma & 0<\gamma<1 \\ t/\ln(t) & \gamma=1 \\ t & \gamma>1. \end{cases} \tag{9}$$

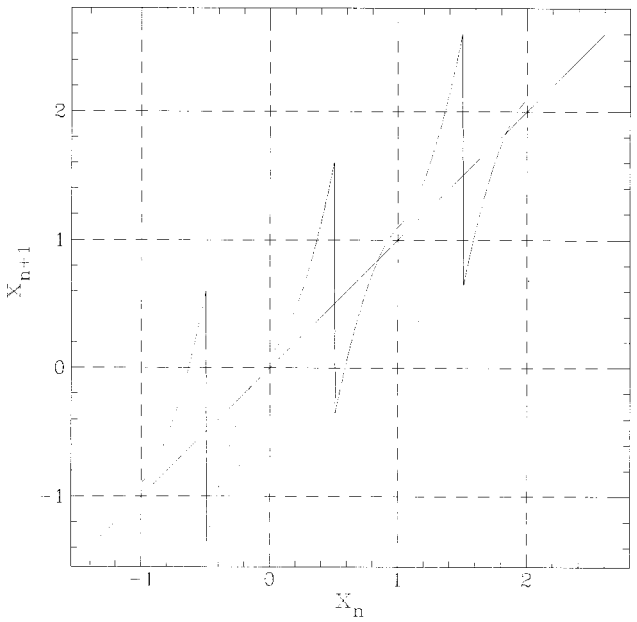

FIG. 1. The map $g(x)+\epsilon$ in the interval $-1<x<2$ for $z=2$ and $a=4$. The field chosen, $\epsilon=0.1$, helps to demonstrate the shifts of the fixed point from their $\epsilon=0$ values.

It should be emphasized that these results are quite general and apply to the class of maps that fulfill Eq. (6). One sees that the exponent z determines the universality class of the diffusion (dispersive or normal diffusion). Notice also that for $0<\gamma<1$ the mean time $\overline{t}=\int_0^\infty t\psi(t)dt$ diverges. Extensive numerical checks of these results were carried out in Refs. [3] and [5].

III. ESCAPE TIME

In this section we treat both analytically and numerically a first passage time problem. We consider a particle located initially close to a fixed point. We then ask how many iterations of the map are needed, so that the particle will cross a boundary. The trajectories which originate in the vicinity of the fixed point are of special interest, since they are responsible for the trapping which is the reason for the slow dynamics that leads to subdiffusion.

The map, defined by Eqs. (1), (3), and (7), has an infinite number of unstable fixed points. Since the map has the periodic shift symmetry defined in Eq. (1), even in the presence of the field, it is enough to consider the fixed point x^* in the vicinity of $x=0$. For $\epsilon \geqslant 0$, the fixed point satisfies

$$x^*=-\left(\frac{\epsilon}{a}\right)^{1/z}\leqslant 0. \tag{10}$$

We assume that the field is weak, so the shift of the fixed point from its integer value is small compared with the size of the box.

Close to the fixed point the increment $x_{n+1}-x_n$ is small, and so we approximate the map by a differential equation

$$\frac{dx}{dt}=f(x)+\epsilon, \tag{11}$$

with $f(x)=g(x)-x$. Such a continuous approximation of the map is common and was used successfully in the theory

of intermittency [17]. Since the fixed point is unstable, a particle initially situated to the right (left) of the fixed point at $x_R(0)>x^*$ [$x_L(0)<x^*$] will flow rightward (leftwards). The time t_R (t_L) it takes a right (left) particle to reach a boundary $b_R>x_R(0)$ [$b_L<x_L(0)$] is

$$t_i=\int_{x_i(0)}^{b_i}\frac{dx}{f(x)+\epsilon}, \tag{12}$$

where $i=L$ or R. In what follows we shall consider first the times t_R.

A. Right escape time

Inserting the explicit expression for $f(x)$ into Eq. (12) we find

$$t_R=\begin{cases}\displaystyle\int_{x_R(0)}^{0}\frac{dx}{-a|x|^z+\epsilon}+\int_0^{b_R}\frac{dx}{a|x|^z+\epsilon}, & x_R(0)<0\\ \displaystyle\int_{x_R(0)}^{b_R}\frac{dx}{a|x|^z+\epsilon}, & x_R(0)\geqslant 0.\end{cases} \tag{13}$$

We define the initial displacement from the fixed point

$$\delta x_R\equiv x_R(0)-x^*>0. \tag{14}$$

The asymptotic behavior of t_R when

$$\left(\frac{a}{\epsilon}\right)^{1/z}\delta x_R\ll 1 \tag{15}$$

is found by the method of integration by parts,

$$t_R\simeq-\frac{1}{z}\epsilon^{(1-z)/z}a^{-1/z}\ln\left[z\left(\frac{a}{\epsilon}\right)^{1/z}\delta x_R\right], \tag{16}$$

exhibiting a logarithmic divergence of the escape time for small initial displacements.

The p.d.f. $\psi_R(t_R)$ of the escape times will be now calculated in a way which is similar to the Geisel and Thomae approach [3]. During the evolution of the system particles are injected close to the vicinity of fixed points. The p.d.f. of the right escape times $\psi_R(t_R)$ is related to the unknown p.d.f. of the injection points $\eta_R[x_R(0)]$, through

$$\psi_R(t_R)=\eta_R[x_R(0)]\left|\frac{dx_R(0)}{dt_R}\right|. \tag{17}$$

The behavior of $\psi_R(t_R)$ at long times is determined by the p.d.f. of the injection points $x_R(0)$ in the vicinity of the fixed point. Expanding $\eta_R[x_R(0)]$ around $x_R(0)=x^*$, and using Eq. (16), we obtain the lowest order approximation,

$$\psi_R(t_R)\sim c_1\exp[-\alpha(\epsilon)t_R], \tag{18}$$

with

$$\alpha(\epsilon)=za^{1/z}\epsilon^{(z-1)/z}. \tag{19}$$

c_1 in Eq. (18) depends on the p.d.f. of injection points. The exponential relaxation of $\psi_R(t_R)$ replaces the power law behavior in the case $\epsilon=0$. This asymptotic behavior of $\psi_R(t_R)$ guarantees that for any small but finite field all moments of the escape times exist. The exponential decay of the p.d.f. is dictated by a relaxation rate $\alpha(\epsilon)$, which becomes smaller as the strength of the bias becomes weaker. It is interesting to note that the exponent $(z-1)/z$, in the expression of the rate [Eq. (19)] is the same exponent that controls the behavior of $\psi_R(t_R)$ in the absence of the bias [see Eq. (8)].

We first assume a uniform density of injection points,

$$\eta_R[x_R(0)]=\begin{cases}\dfrac{1}{b-x^*}, & x^*<x_R(0)<b\\ 0, & \text{otherwise.}\end{cases} \tag{20}$$

For this choice, the averaged time $\langle t_R\rangle$ scales according to

$$\left\langle t_R a^{1/z}\epsilon^{(z-1)/z}\right\rangle=G_z(y_R), \tag{21}$$

where

$$y_R\equiv\frac{b_R}{|x^*|} \tag{22}$$

is a dimensionless variable. The scaling function $G_z(y_R)$ depends on the exponent z which determines the universality class of the diffusion. This relationship is useful for scaling representation of data. To see why this scaling form is correct we rewrite Eq. (13) as

$$t_R a^{1/z}\epsilon^{(z-1)/z}=H(x_R,y_R), \tag{23}$$

with the dimensionless initial condition

$$x_R\equiv\frac{x_R(0)}{|x^*|}, \tag{24}$$

and with

$$H(x_R,y_R)=\int_{x_R}^{0}\frac{dw}{-|w|^z+1}+\int_0^{y_R}\frac{dw}{|w|^z+1}$$

for $-1<x_R<0$, and

$$H(x_R,y_R)=\int_{x_R}^{y_R}\frac{dw}{|w|^z+1} \tag{25}$$

for $0\leqslant x_R<y_R$. We then integrate Eq. (23), using Eq. (20), and obtain the scaling result [Eq. (21)] with the scaling function

$$G_z(y_R)=\frac{1}{y_R+1}\int_{-1}^{y_R}dw\ H(w,y_R). \tag{26}$$

The scaling relation [Eq. (21)] has been derived using the assumption of a uniform injection of particles. In the Appendix, we give a more general condition on the p.d.f. of injection points for which scaling holds.

We now investigate the field dependence of $\langle t_R\rangle$, since both the drift $\langle x(t)\rangle$ and the mean squared displacement $\langle x^2(t)\rangle$ depend on the mean escape time. Integrating by parts the left hand side of Eq. (21), we find

$$\langle t_R\rangle = \frac{1}{a^{1/z}\epsilon^{(z-1)/z}}\frac{1}{1+y_R}\left(\int_0^{y_R}\frac{w+1}{w^z+1}dw+\int_0^1\frac{1-w}{1-w^z}dw\right). \tag{27}$$

The asymptotic behavior of $\langle t_R\rangle$, when $y_R \gg 1$, depends on z.

For values $z>2$, which in the absence of the field correspond to dispersive diffusion,

$$\langle t_R\rangle \simeq \frac{1}{\epsilon^{(z-2)/z}}\frac{C_z}{b_R a^{2/z}}, \tag{28}$$

with the numerical factor

$$C_z = \int_0^\infty \frac{w+1}{w^z+1}dw+\int_0^1\frac{1-w}{1-w^z}dw. \tag{29}$$

For $z<2$, for which diffusion is normal, we find

$$\langle t_R\rangle \simeq \frac{1}{(2-z)b_R^{z-1}a}, \tag{30}$$

and, for the intermediate case $z=2$,

$$\langle t_R\rangle \simeq \frac{\ln\left[b_R\left(\frac{a}{\epsilon}\right)^{1/2}\right]}{b_R a}. \tag{31}$$

Notice that when $z<2$, $\langle t_R\rangle$ is independent of the weak field. This result is expected since $\langle t_R\rangle$, when $\epsilon=0$, exists. For $z>2$ and $\epsilon=0$, $\langle t_R\rangle$ does not exist. Equation (28) shows that for small fields $\langle t_R\rangle$ diverges as a power law with the exponent $(z-2)/z$.

B. An example

We now consider the special case $z=2$, and analyze it in some detail. This choice enables us to find the analytical expression for the p.d.f. $\psi_R(t_R)$.

Integrating Eq. (13) and using a table of integrals [18], we find

$$t_R = \frac{1}{\sqrt{\epsilon a}}\left\{-\operatorname{arctanh}\left[\frac{x_R(0)}{|x^*|}\right]+\arctan\left(\frac{b_R}{|x^*|}\right)\right\}$$

for $x^*<x_R(0)<0$, and

$$t_R = \frac{1}{\sqrt{\epsilon a}}\left\{-\arctan\left[\frac{x_R(0)}{|x^*|}\right]+\arctan\left(\frac{b_R}{|x^*|}\right)\right\} \tag{32}$$

for $0<x_R(0)<b_R$. Here

$$\operatorname{arctanh}(x)=\frac{1}{2}\ln\left(\frac{1+x}{1-x}\right) \quad \text{for } [-1<x<1].$$

Averaging t_R over the uniform injection p.d.f. Eq. (20) gives [18]

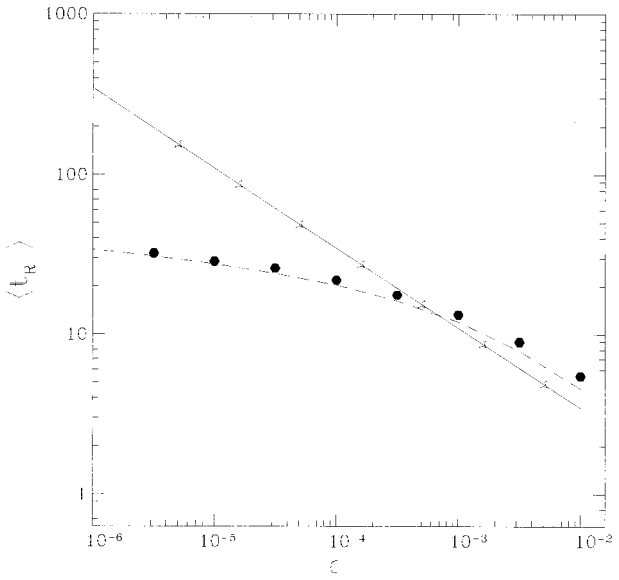

FIG. 2. The escape time $\langle t_R\rangle$ for two choices of the location of the boundary b_R. Each point is found after averaging over 40 000 escape events. The solid curve ($b_R=0$) is the theoretical result in Eq. (34). The dashed curve ($b_R=0.05$) is the result in Eq. (31). Here $a=4$.

$$\langle t_R\rangle = \frac{1}{\sqrt{\epsilon a}}\frac{1}{1+\frac{b_R}{|x^*|}}\left\{\ln(2)+\arctan\left(\frac{b_R}{|x^*|}\right)+\frac{1}{2}\ln\left[1+\left(\frac{b_R}{|x^*|}\right)^2\right]\right\}. \tag{33}$$

The behavior of $\langle t_R\rangle$ strongly depends on the location of the boundary b_R. When $b_R=0$,

$$\langle t_R\rangle = \frac{\ln(2)}{\sqrt{\epsilon a}}, \tag{34}$$

while when

$$y_R=\frac{b_R}{|x^*|}=\frac{b_R\sqrt{a}}{\sqrt{\epsilon}}\gg 1, \tag{35}$$

Eq. (31) is valid. Both Eqs. (31) and Eq. (34) show a divergence of $\langle t_R\rangle$ as $\epsilon\to 0$. However, the location of the boundary b_R determines the type of divergence.

We have checked these predictions numerically using the recursion relation [Eq. (7)]. The trajectory of a particle has been followed, and once it passed a fixed boundary it was reinjected randomly and uniformly back into the interval $x^*<x<b_R$. In Fig. 2 we plot $\langle t_R\rangle$ vs ϵ on a log-log scale. We have chosen two boundary conditions: $b_R=0$, for which Eq. (34) applies, and $b_R=0.05$, for which Eq. (31) applies. The results of the numerical experiment are in good agreement with the analytical derivations. Deviations are noticed for the field $\epsilon=0.01$. We believe these deviations are caused by the discrete nature of the map which cannot be overlooked when ϵ becomes large and simultaneously $\langle t_R\rangle$ becomes smaller. When iterating the map the escape times ob-

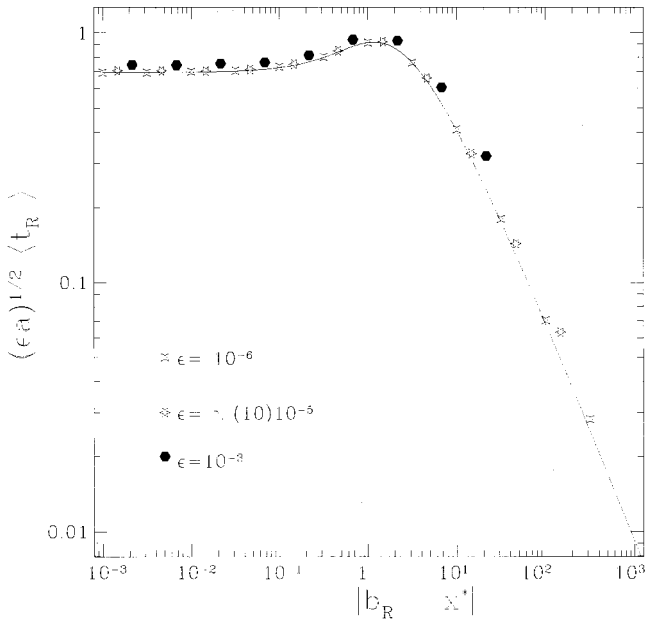

FIG. 3. The scaled averaged time $\sqrt{\epsilon a}\langle t_R\rangle$ vs the scaled boundary condition $|b_R/x^*|$ is displayed for three values of the field. Varying the location of the boundary in the range $0<b_R<0.5$ we find numerically the averaged time of escape. Each point is the average over 40 000 escape events.

tain integer values, while the escape times, when calculated with the differential equation, are continuous. Therefore for short escape times the differential equation is not a good approximation for the iterated map. Another cause for disagreement between theory and numerical calculation arises when iterations are performed far from the fixed point. Then the difference $x_{n+1}-x_n$ is not small, as can be seen in Fig. 1. Iterations far from the fixed point enter when b_R is large, a case for which the differential equation approximation is not expected to be valid.

In Fig. 3 we display the scaled averaged time and check the scaling behavior numerically. The curve plotted is the theoretical prediction given by Eq. (33). When $y_R<1$, the scaled averaged time behaves as a constant, while when $y_R>1$ it decreases as predicted by Eq. (31). Scaling is observed to hold well for weak fields. Small deviations are found when the strength of the field is $\epsilon=10^{-3}$; for this case the differential equation is not such a good approximation for the recursion relation.

For the case $z=2$, one obtains an exact expression for the p.d.f. of the escape times. Using Eq. (17), we find

$$\psi_R(t_R)=\frac{\epsilon}{b_R-x^*}\frac{1}{\cos^2[t_R\sqrt{\epsilon a}-\phi_R]} \quad \text{for } t_R<t_{\text{tran}}, \tag{36}$$

$$\psi_R(t_R)=\frac{\epsilon}{b_R-x^*}\frac{1}{\cosh^2[t_R\sqrt{\epsilon a}-\phi_R]} \quad \text{for } t_{\text{tran}}<t_R, \tag{37}$$

with the phase

$$\phi_R=\arctan\left(\frac{b_R}{|x^*|}\right),$$

and the transition time

$$t_{\text{tran}}=\frac{\arctan\left(\dfrac{b_R}{|x^*|}\right)}{\sqrt{\epsilon a}}, \tag{38}$$

which gives the crossover time between the two different types of behaviors of the p.d.f. When $b_R/|x^*|\gg 1$, the transition time diverges according to

$$t_{\text{tran}}\simeq\frac{\pi}{2\sqrt{\epsilon a}}. \tag{39}$$

When $b_R=0$, $t_{\text{tran}}=0$, and the p.d.f. decays according to Eq. (37). For long times, $t\gg t_{\text{tran}}$, the p.d.f. decays exponentially

$$\psi_R(t_R)\sim\exp(-2t\sqrt{\epsilon a}), \tag{40}$$

as predicted in Eq. (18). As mentioned, this behavior guarantees that for finite ϵ all the moments of the p.d.f. exist.

In the limit $\epsilon\to 0$ (b_R finite), we obtain the p.d.f.

$$\lim_{\epsilon\to 0}\psi_R(t_R)=\frac{b_R a}{(1+b_R a t_R)^2}, \tag{41}$$

showing the expected power law dependence for long times $\psi_R(t_R)\sim t_R^{-2}$, and the divergence of the moments of t_R. This behavior was anticipated in previous works which considered the case $\epsilon=0$ [set $b_R=0.5$ in Eq. (41) and obtain Eq. (8)]. It is interesting to compare the p.d.f. when $\epsilon\to 0$ to the p.d.f. when the field is finite but small. This is done in Fig. 4, where the p.d.f. is shown for three different fields using Eqs. (36) and (37), as well as the result in Eq. (41). One sees that when $t\ll t_{\text{tran}}$ all four curves converge to a single curve. Hence the behavior of the p.d.f. for times shorter then the transition time t_{tran} follows a power law. To determine the correct asymptotic behavior of the p.d.f. it is useful to know the transition time. This means that measuring the escape times (say numerically) for not long enough observation times, might lead to the wrong conclusion that the p.d.f., even in the presence of the field, behaves like a power law.

The above behavior is observed numerically in Fig. 5, where the p.d.f. is plotted for the special case $\epsilon=4\times10^{-6}$. The boundary b_R has been chosen to satisfy $b_R/|x^*|=1$. One observes good agreement between theory and the numerical results. In Fig. 6 a log-log plot of the p.d.f. is shown, and a power law behavior is observed when $t<t_{\text{tran}}$. Here the boundary has been chosen to satisfy $b_R/|x^*|=500$. For very short times, deviations between theory and numerical data exist due to the discrete nature of the map. For very long times one notices the exponential behavior of the p.d.f.

We also carried out numerical experiments without using the uniform injection of particles to the vicinity of the fixed point. An ensemble of trajectories was produced. The initial conditions of these trajectories were distributed uniformly in the interval (0,1). For each initial condition the map was

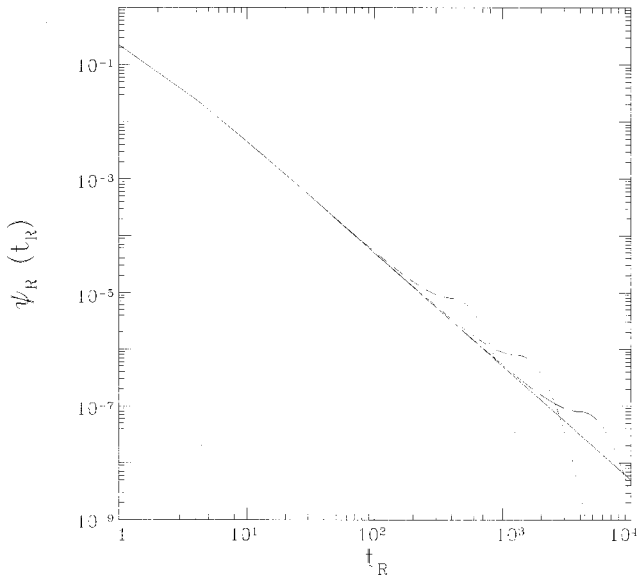

FIG. 4. The p.d.f. $\psi_R(t_R)$ on a log-log scale. The solid curve corresponds to $\lim_{\epsilon\to 0}\psi_R(t_R)$. The other three curves give $\psi_R(t_R)$ (a) $\epsilon=4\times10^{-6}$, the short dashed line; (b) $\epsilon=4\times10^{-7}$, the dash dotted line; and (c) $\epsilon=4\times10^{-8}$, the long dashed line. As the field strength is decreased, the transition time to the exponential behavior of the p.d.f. becomes longer. Here the boundary is $b_R=0.5$.

iterated for times t satisfying $t>t_{\text{tran}}$. Then we continued to iterate the map until the particle was injected in the vicinity of a fixed point. The trajectory was followed until the particle crossed a boundary. In this case the injection p.d.f. is not assumed to be uniform, and may have a structure that depends on the details of the map. This method has the disadvantage of being numerically less efficient as compared with the previous method. However, the p.d.f. obtained in this way mimics in a better way the p.d.f, we encounter in the transport process.

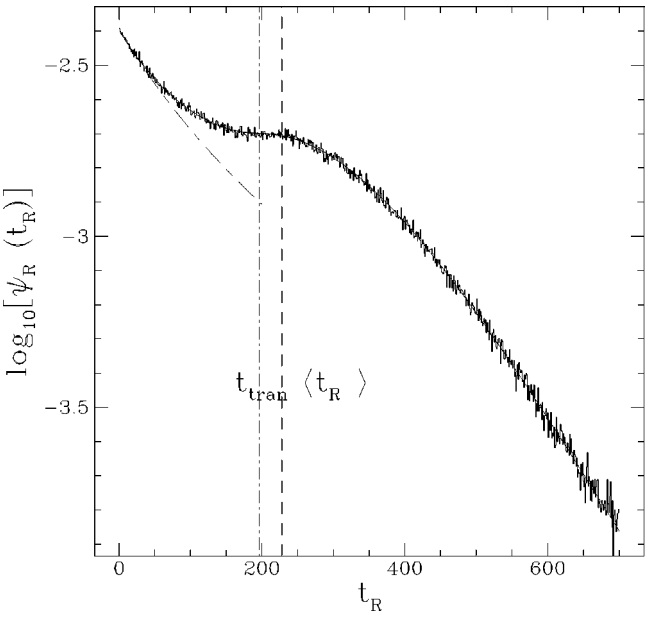

FIG. 5. The p.d.f. $\psi_R(t)$ for a boundary value $b_R=0.001$. Here $\epsilon=4\times10^{-6}$ and $a=4$, and therefore, $x^*=-0.001$. The transition time and the averaged escape time are indicated by the dot-dashed and dashed vertical lines respectively. For $t_R>t_{\text{tran}}$ the linearity of the curve indicates the exponential relaxation. For $t_R<t_{\text{tran}}$ we also plot $\lim_{\epsilon\to 0}\psi_R(t_R)$, Eq. (41). The bin length for the histogram is unity. 10^6 escaped times were recorded.

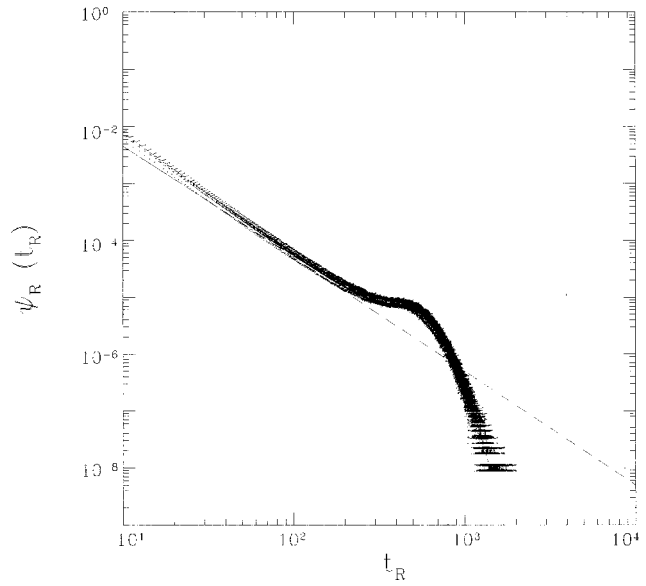

FIG. 6. The p.d.f. $\psi_R(t_R)$ on a log-log plot. Here the boundary $b_R=0.5$. The dashed line is the limit $\epsilon\to0$ of the p.d.f. The dot-dashed line is the theoretical curve. 10^8 escaped times were recorded.

In Fig. 7, we present the p.d.f. for the field $\epsilon=10^{-4}$. Notice that for long times the p.d.f decays exponentially with time. Good agreement is observed between the numerically calculated points and the theoretical curve calculated under the assumption of a uniform injection. Figure 8 displays the data on a log-log plot for the case $\epsilon=4\times10^{-6}$. We have

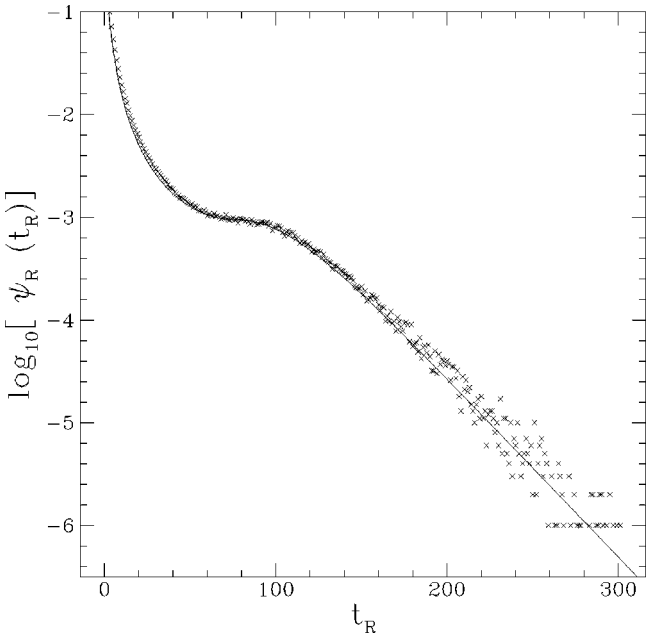

FIG. 7. Using the map Eq. (7), we find the p.d.f. of right escape times. The boundary is located at $b=0.1$, the number of realizations is 10^6, and $\epsilon=10^{-4}$. The solid curve is the theoretical prediction in Eq. (37).

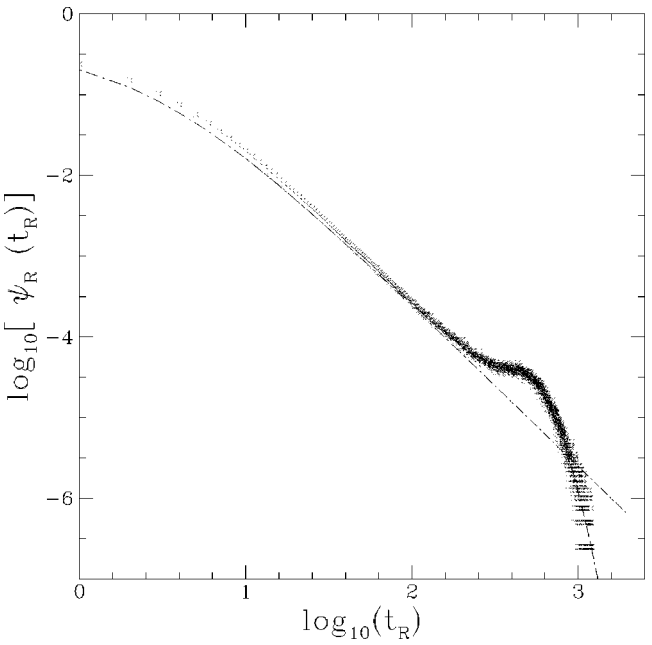

FIG. 8. The p.d.f. on a log-log plot for the bias $\epsilon=4\times10^{-6}$, and $b=0.1$. The number of realizations is 4×10^{6}. The dashed line is the theoretical prediction in Eq. (37). The dot-dashed line is the limit $\epsilon\to0$ of the p.d.f. Eq. (41). As shown in Fig. 4, choosing a smaller value of ϵ increases the time window in which the power law behavior is observed.

also plotted the theoretical prediction in the limit $\epsilon\to0$. For times $t<t_{\rm tran}$, we see that the p.d.f behaves as a power law, while for $t>t_{\rm tran}$ the exponential decay is observed. The injection p.d.f obtained numerically for our choice of parameters is found to be quite flat, which explains the good agreement between the theory and the numerical calculation.

C. Left escape time

The bias ϵ breaks the symmetry of the map and therefore the left escape time t_L behaves differently than t_R. The following results for the left escape time have been derived in a similar way to those obtained for the right escape time. Using Eq. (12),

$$t_L=\int_{x_L(0)}^{b_L}\frac{dx}{-a|x|^z+\epsilon}$$

with

$$b_L<x_L(0)<x^*<0. \tag{42}$$

We define the initial displacement from the fixed point

$$\delta x_L\equiv x_L(0)-x^*<0, \tag{43}$$

and find the asymptotic behavior of t_L

$$t_L\simeq-\frac{1}{z}\epsilon^{(1-z)/z}a^{-1/z}\ln\left[z\left(\frac{a}{\epsilon}\right)^{1/z}|\delta x_L|\right], \tag{44}$$

which is exactly the same behavior found for the escape time t_R. This means that the asymptotic, large t_L, behavior of the p.d.f. of the escape times $\psi_L(t_L)$ decays exponential with the rate $\alpha(\epsilon)$ defined in Eq. (19). To obtain the asymptotic dependence of $\langle t_L\rangle$ on ϵ, we again use a uniform injection of particles,

$$\eta_L[x_L(0)]=\begin{cases}\dfrac{1}{x^*-b_L}, & b_L<x_L(0)<x^*\\ 0, & \text{otherwise.}\end{cases} \tag{45}$$

Using this p.d.f. for averaging t_L, we find

$$\langle t_L\rangle=\epsilon^{(1-z)/z}a^{-1/z}\frac{1}{y_L-1}\int_1^{y_L}\frac{w-1}{w^z-1}dw, \tag{46}$$

with

$$y_L\equiv|b_L|\left(\frac{a}{\epsilon}\right)^{1/z}. \tag{47}$$

When $y_L\gg1$, three types of asymptotic behaviors are found:

$$\langle t_L\rangle\simeq\begin{cases}\dfrac{1}{\epsilon^{(z-2)/z}}\dfrac{1}{|b_L|a^{2/z}}\displaystyle\int_1^{\infty}\frac{x-1}{x^z-1}dx, & z>2\\ \dfrac{\ln\left[|b_L|\left(\frac{a}{\epsilon}\right)^{1/2}\right]}{|b_L|a}, & z=2\\ \dfrac{1}{(2-z)|b_L|^{z-1}a}, & z<2.\end{cases} \tag{48}$$

These asymptotic results show that for $z\leqslant2$, $\langle t_L\rangle=\langle t_R\rangle$ when $|b_L|=b_R$.

The p.d.f. of the left escape times for $z=2$ is

$$\psi_L(t_L)=\frac{\epsilon}{-b_L+x^*}\frac{1}{\sinh^2(\sqrt{\epsilon a}t_L+\phi_L)}, \tag{49}$$

with the phase

$$\phi_L=\operatorname{arccoth}\left(\frac{|b_L|}{|x^*|}\right).$$

In the limit $\epsilon\to0$, we find

$$\lim_{\epsilon\to0}\psi_L(t)=\lim_{\epsilon\to0}\psi_R(t) \tag{50}$$

where $\lim_{\epsilon\to0}\psi_R(t)$ is given in Eq. (41).

We see that although the left and right times are not identical, the p.d.f.'s $\psi_R(t)$ and $\psi_L(t)$ share some common features: the long time behavior, the ϵ dependence of the averaged escape times when ϵ is small, and the approach to a power law behavior when $\epsilon\to0$ (here shown only for $z=2$).

IV. MEAN AND MEAN SQUARED DISPLACEMENTS

The mean displacement $\langle x(t)\rangle$ and the mean squared displacement $\sigma^2(t)=\langle x^2(t)\rangle-\langle x(t)\rangle^2$ are now investigated. In Fig. 9 we present a typical trajectory of the particle obtained

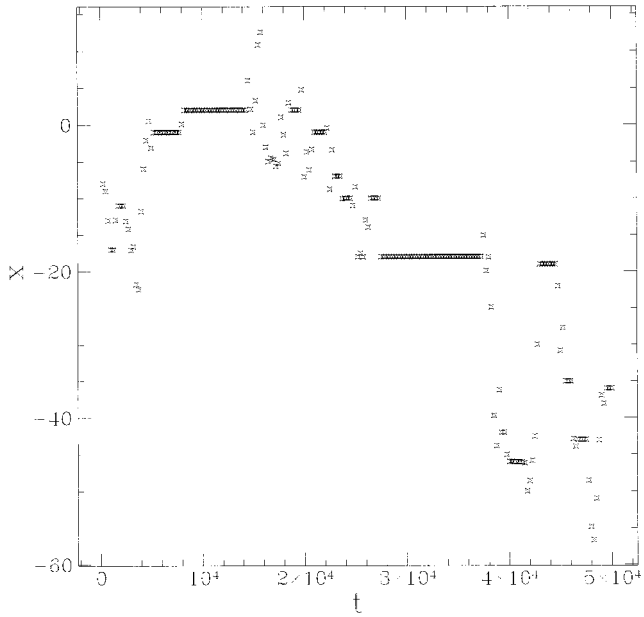

FIG. 9. A typical trajectory resulting from 4×10^4 iterations of the map for the parameters $z=2$, $a=4$, and $\epsilon=0$.

from a numerical iteration of the map for the case $z=2$ and $\epsilon=0$. We notice that the particle is trapped for long periods of time. The trapping occurs close to fixed points. In Fig. 10 a trajectory is presented for $\epsilon=0.001$. The initial condition for this trajectory is identical to the one chosen for the trajectory considered in Fig. 9; however, now one does not observe long trapping events. Also seen in Fig. 10 is a net drift in the direction of the applied field. The difference between Figs. 9 and 10 is a manifestation of the difference in the p.d.f.'s $\psi_R(t)$ and $\psi_L(t)$ with and without a field [Eqs. (8) and (18)].

It has been shown that, at least, for the case $\epsilon=0$ [3,5] the CTRW can be used to describe the statistical properties of the dynamics of the map. The CTRW model describes a particle hoping from site to site and pausing at each site [19,20]. The main result of the CTRW theory, relevant to our

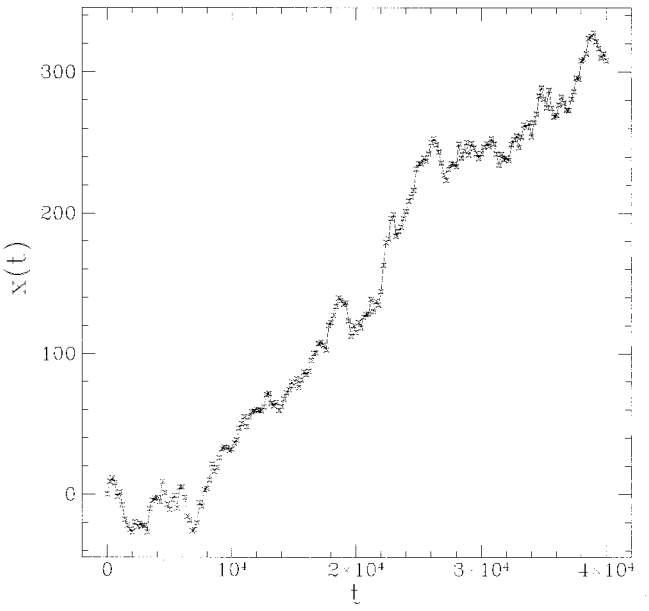

FIG. 10. Same as Fig. 9, for a bias $\epsilon=0.001$.

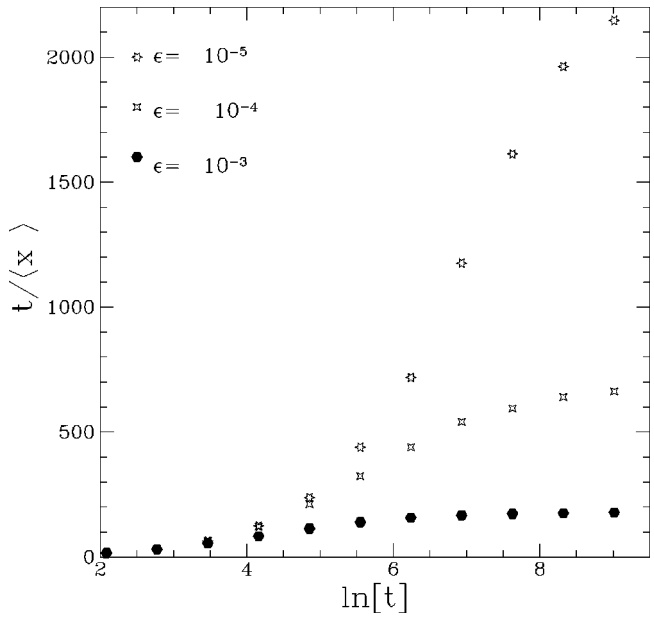

FIG. 11. $t/\langle x(t)\rangle$ vs $\ln(t)$ for different values of the bias ϵ. Here $z=2$ and $a=4$, and the average is over 10^6 realizations.

work here, is that, when the averaged pausing time $\langle\tau\rangle$, the averaged length of the displacement $\langle\tilde{x}\rangle$, and $\langle\tilde{x}^2\rangle$ exist, then, for long times,

$$\langle x(t)\rangle \simeq \frac{\langle\tilde{x}\rangle}{\langle\tau\rangle}t \tag{51}$$

and

$$\langle\sigma^2(t)\rangle \simeq 2Dt, \tag{52}$$

with the diffusion constant

$$D=\frac{\langle\tilde{x}^2\rangle}{2\langle\tau\rangle}. \tag{53}$$

Equations (51) and (53) do not hold when $\langle\tau\rangle$ diverges, that is, when $\epsilon=0$ and $z\geqslant 2$ [3].

We define the pausing time, $\tau\equiv t_L$ ($\tau\equiv t_R$) if the particle is injected to the left (right) of a fixed point. Then the averaged pausing, or escape, time is

$$\langle\tau\rangle = P_L\langle t_L\rangle + P_R\langle t_R\rangle, \tag{54}$$

where P_L (P_R) is an unknown probability, in an ongoing process, that a particle will be injected to the vicinity of a fixed point and flow to left (right). Using this approach we can reach several qualitative conclusions.

Since we have shown that the averaged escape times $\langle t_R\rangle$ and $\langle t_L\rangle$ exist [Eqs. (27)–(30) and (45) for finite ϵ], then, according to Eqs. (51) and (52), the mean displacement and mean squared displacement increase linearly with time when $\epsilon\neq 0$. Thus dispersive diffusion found for $\epsilon=0$ turns into normal diffusion for any small though finite ϵ.

This type of behavior is observed in our numerical simulations carried out for the special case $z=2$. The initial conditions of these trajectories have been distributed uniformly in the interval (0,1). Averages have been taken over 10^6 realizations. In Fig. 11 the $t/\langle x(t)\rangle$ vs $\ln(t)$ curve shows that

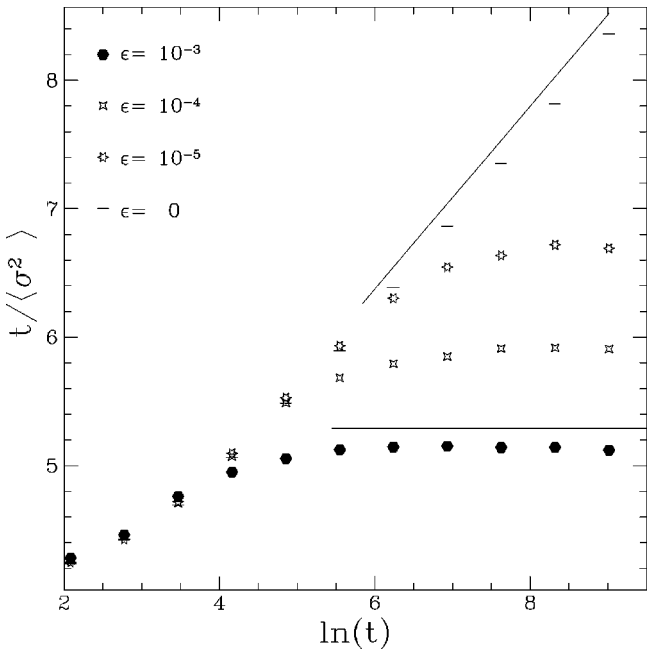

FIG. 12. $t/\langle\sigma^2(t)\rangle$ vs $\ln(t)$ for different values of the bias. Other parameters of the map are specified in Fig. 11. The predicted asymptotic slopes are shown for two cases.

for short times $\langle x(t)\rangle$ is a nonlinear function of time. For long times $t/\langle x(t)\rangle$ is a constant independent of $\ln(t)$. This can be seen best for the curve which corresponds to $\epsilon=0.001$, where the transition time from dispersive to normal type of behaviors is relatively short.

The transition from dispersive to normal type of motion can be observed better when considering the mean squared deviation $\langle\sigma^2(t)\rangle$. In Fig. 12, $t/\langle\sigma^2(t)\rangle$ vs $\ln(t)$ is displayed for different fields. Two kinds of behaviors are found: (1) For $\epsilon=0$ a linear curve is found meaning that $\sigma^2(t)\sim t/\ln(t)$, as predicted in Eq. (9) and observed previously in Ref. [3]. (2) For $\epsilon=0.001$, the behavior $\sigma(t)\sim t$ is found for long times as predicted in Eq. (52). One sees that the larger is the applied field the shorter is the transition time to normal behavior.

In order to find the field dependence of the diffusion, we notice that

$$D\sim\frac{1}{\langle\tau(\epsilon)\rangle}, \tag{55}$$

since $\lim_{\epsilon\to 0}\langle\tilde{x}^2\rangle$ is finite and independent of ϵ. Clearly, due to symmetry, for very weak fields,

$$P_R=0.5+\xi(\epsilon)\quad\text{and}\quad P_L=0.5-\xi(\epsilon), \tag{56}$$

where $\xi(\epsilon)$ is small. We find, using Eqs. (29)–(31), (48), and (56), that, for weak fields,

$$D\sim\begin{cases}\text{const}, & z<2\\ 1/|\ln\sqrt{\epsilon}|, & z=2\\ \epsilon^{(z-2)/z}, & z>2,\end{cases} \tag{57}$$

independent of $\xi(\epsilon)$. As expected, for $z<2$, the diffusion constant is independent of ϵ (since we know that D is finite when $\epsilon=0$). For $z>2$ the diffusion constant, which vanishes when $\epsilon=0$, shows a power law dependence on the weak external field. The results in Eq. (57) are derived here within a space-time decoupled scheme of the CTRW. The same results, however, are obtained when coupling is assumed in the limit of $\epsilon\to 0$ [21].

The dependence of $\langle x(t)\rangle$ on ϵ cannot be determined in a similar way since we do not know the ϵ dependence of $\langle\tilde{x}\rangle$ in Eq. (51). This question has to do with the response of these maps to an external bias, a subject we plan to check numerically. Thus our results can be used to predict a linear dependence of $\langle x(t)\rangle$ on t, but not the response of $\langle x(t)\rangle$ to the field.

An important issue is the relation between drift and diffusion in deterministic systems. This issue has been tackled previously in a somewhat similar context by Trefán and coworkers [13–15]. One might expect the Green Kubo relation [22] and the generalized Einstein relation [23] to determine the relationship between the drift and diffusion. The generalized Einstein relation states that the response $\langle x(t)\rangle_\epsilon$ of the particles to an external weak and uniform field ϵ obeys

$$\langle x(t)\rangle_\epsilon=k_1\epsilon\langle x^2(t)\rangle_{\epsilon=0}, \tag{58}$$

where $\langle x^2(t)\rangle_{\epsilon=0}$ is the mean squared displacement of the particles with no bias and k_1 is a constant. The theoretical basis for this relation is a linear response to the external field. However, numerical simulations [21] show that the response ($\langle x\rangle$) to the external field is nonlinear. Therefore the Einstein approach cannot be used. Furthermore, for long times $\langle x(t)\rangle$ increases linearly with time when $\epsilon\neq 0$, while Eq. (9) shows that $\langle x^2\rangle_{\epsilon=0}$ may increase nonlinearly with time and so clearly the generalized Einstein relation [Eq. (58)] fails to describe the transport generated by the maps.

V. SUMMARY

The results of adding bias to deterministic systems, which lead to regular or anomalous diffusion, depend on the nature of the applied field and on the underlying system. Bias can therefore be used to control transport properties of such systems by changing the motion from anomalous to regular and vice versa. Studying ways to introduce bias, and analyzing systems under applied fields, have been growing research areas [13–15,10,24,25] Ishizaki and Mori [24] investigated the forced standard map, the Josephson map, and demonstrated a transition from regular to anomalous transport. A model to explain the tracer diffusion experiments of Swinney and co-workers [9,10] was proposed by del-Castillo-Negrete [25]. The model leads to anomalous diffusion under bias.

Here the effect of an external field on one-dimensional maps which generate deterministic diffusion has been investigated both analytically and numerically. A weak uniform bias breaks the symmetry of the system and leads therefore to a net averaged drift. We have shown that the p.d.f. of the escape times is sensitive to the field. When the field is switched on, right and left escape times become nonidentical. The p.d.f. in the absence of the field follows a power law. In the presence of the weak uniform field the the p.d.f. decays exponentially for large times. The rate of decay of the p.d.f.'s $\alpha(\epsilon)$, given in Eq. (19), approaches zero as a power law in the field for all values of z. Since the power law

behavior of the p.d.f. manifests itself in anomalous diffusion when $z \geqslant 2$, the presence of the field destroys this behavior >and regular transport appears at long times for all z.

Trefán and co-workers [13–15] previously considered the influence of a perturbation on closely related maps which generate enhanced diffusion. They considered both a dynamical bias and geometrical bias (see details in Ref. [13]). Under their assumptions the motion may cross over from enhanced to regular. The drift is introduced in their approach by assuming two different waiting time p.d.f.'s (left and right). This is obtained by driving the left laminar region with the perturbed map [Eq. (6)] with a nonvanishing λ. In the current work the field is homogeneous; the bias leads to a shift of the fixed points and to the breakdown of symmetry. The perturbation considered by Trefán and co-workers leads to a waiting time p.d.f.,

$$\lim_{t\to\infty} \psi_T(t) \sim \frac{\exp(-c_1 \lambda t)}{t^{\mu}}, \tag{59}$$

where c_1 is a constant. The rate of the exponential decay grows linearly with the perturbation λ. This is different from our result [Eq. (18)], where the rate $\alpha(\epsilon)$ [Eq. (19)] increases nonlinearly with ϵ.

APPENDIX

Here we give the more general condition on $\eta_R[x_R(0)]$ for which scaling exists, with a scaling function $\widetilde{G}_z(y_R)$ which may differ from the function $G_z(y_R)$. A straightforward change of variables in Eq. (25) leads to

$$\left\langle t_R a^{1/z} \epsilon^{(z-1)/z} \right\rangle = |x^*| \int_{-1}^{y_R} d\beta \ \eta_R(\beta |x^*|) H(\beta, y). \tag{A1}$$

It follows immediately that if a dimensionless function $f(\beta, y_R)$ exists, such that

$$|x^*| \, \eta_R(\beta |x^*|) = f(\beta, y_R), \tag{A2}$$

then we find the scaling relation

$$\left\langle t_R a^{1/z} \epsilon^{(z-1)/z} \right\rangle = \int_{-1}^{y_R} d\beta \ f(\beta, y_R) H(\beta, y_R) \equiv \widetilde{G}_z(y_R). \tag{A3}$$

Functions that satisfy the condition in Eq. (A2) are the p.d.f.'s which scale like

$$\eta_R[x_R(0)] = \frac{1}{L} \overline{\eta}_R \left[\frac{x_R(0)}{L} \right] \ \text{with} \ L \equiv |x^*| + b_R; \tag{A4}$$

here $\overline{\eta}_R(x)$ is a dimensionless function of x. The prefactor $1/L$ guarantees that $\eta_R[x_R(0)]$ has the units $[\text{Length}]^{-1}$. To see this, we use Eq. (A4) and obtain

$$|x^*| \, \eta_R(\beta |x^*|) = \frac{1}{1+y_R} \overline{\eta}_R \left(\frac{\beta}{1+y_R} \right), \tag{A5}$$

which clearly satisfies the condition in Eq. (A2). That is, when the p.d.f. $\eta_R[x_R(0)]$ scales with L in a way defined in Eq. (A4), the scaling relation Eq. (A3) for the mean escape time exists. L is the length of the interval into which particles are injected. In an ongoing process particles are injected from cell to cell. Injection events occur from points far from the fixed point. The scaling will work well when the injection p.d.f. depends on the single length scale L. It should be noted that the injection probability depends on the global details of the map and not only on the behavior close to the fixed point, which means that scaling depends on the model under consideration.

[1] J. Klafter, M. F. Shlesinger, and G. Zumofen, Phys. Today **49**, 33 (1996).

[2] *Lévy Flights and Related Topics in Physics*, edited by M. F. Shlesinger, G. M. Zaslavsky, and U. Frisch (Springer-Verlag, Berlin, 1994).

[3] T. Geisel and S. Thomae, Phys. Rev. Lett. **52**, 1936 (1984).

[4] T. Geisel, J. Nierwetberg, and A. Zacherl, Phys. Rev. Lett. **54**, 616 (1985).

[5] G. Zumofen and J. Klafter, Phys. Rev. E **47**, 851 (1993).

[6] G. Zumofen and J. Klafter, Physica D **69**, 436 (1993).

[7] G. Zumofen and J. Klafter, Physica A **196**, 102 (1993).

[8] G. Zumofen and J. Klafter, Phys. Rev. E **51**, 1818 (1995).

[9] T. H. Solomon, E. R. Weeks, and H. L. Swinney, Phys. Rev. Lett. **71**, 23 (1995).

[10] R. Weeks, J. S. Urbach, and H. L. Swinney, Physica D **97**, 291 (1996).

[11] R. Bettin, R. Mannella, B. J. West, and P. Grigolini, Phys. Rev. E **51**, 212 (1995).

[12] G. Radons, Phys. Rev. Lett. **77**, 23 (1996).

[13] G. Trefán, E. Floriani, B. J. West, and P. Grigolini, Phys. Rev. E **50**, 2564 (1994).

[14] E. Floriani, G. Trefán, P. Grigolini, and B. J. West, in *Levy Flights and Related Topics in Physics* (Ref. [2]).

[15] E. Floriani, G. Trefán, P. Grigolini, and B. J. West, Phys. Lett. A **218**, 35 (1996).

[16] H. G. Schuster, *Deterministic Chaos: An Introduction* (Physic Verlag, Weinheim, 1984).

[17] J. E. Hirsch, B. A. Huberman, and D. J. Scalapino, Phys. Rev. E **25**, 519 (1982).

[18] I. S. Gradshteyn and I. M. Rhyzik, *Tables of Integrals, Series, and Products* (Academic, New York, 1980).

[19] E. W. Montroll and G. H. Weiss, J. Math. Phys. **6**, 167 (1965).

[20] E. W. Montroll and M. F. Shlesinger, in *Nonequilibrium Phenomena II, From Stochastics To Hydrodynamics*, edited by J. L. Lebowitz and E. W. Montroll (North-Holland, Amsterdam, 1984).

[21] E. Barkai and J. Klafter, Phys. Rev. Lett. **79**, 2245 (1997).

[22] R. Kubo, M. Toda, and N. Hashitsume, *Statistical Physics 2* (Springer-Verlag, Berlin, 1991).

[23] J. P. Bouchaud and A. Georges, Phys. Rep. **195**, 127 (1990).

[24] R. Ishizaki and H. Mori, Prog. Theor. Phys. **97**, 201 (1997).

[25] D. del-Castillo-Negrete, J. Fluids (to be published).